

Understanding the Difference in Oxidative Properties between Flame and Diesel Soot Nanoparticles: The Role of Metals

S. H. KIM, R. A. FLETCHER, AND
M. R. ZACHARIAH*

Nanoparticle-Based Manufacturing and Metrology Laboratory, Departments of Mechanical Engineering and Chemistry, University of Maryland, College Park, Maryland 20742, and National Institute of Standards and Technology, Gaithersburg, Maryland 20899

The purpose of this paper is to address the differences observed in the oxidative kinetics between flame and diesel derived soots. In particular, it has been observed that flame soot has a significantly higher activation energy for oxidation than does diesel soot. The hypothesis tested in this paper is that metals, possibly coming from lubricating oils, within diesel generated soot particles may be responsible for this effect. This is supported by the fact that addition of metal additives to diesel fuel is shown to have no effect on the activation energy of soot oxidation. The subject of this paper lies in testing the hypothesis by adding metal directly to a flame and extracting oxidation kinetics. Using a high temperature oxidation tandem differential mobility analyzer (HTO-TDMA) we extract particle size dependent kinetics for the oxidation of flame-derived soot doped with and without iron. We found that indeed addition of iron to a flame reduced the activation energy significantly from $\sim 162 \pm 3$ kJ/mol to $\sim 116 \pm 3$ kJ/mol, comparable with diesel engine generated soot with an activation energy ~ 110 kJ/mol. These results are consistent with the idea that small quantities of metals during diesel combustion may play an important role in soot abatement.

Introduction

The particulate emission from power sources is generally in the form of carbonaceous soot produced by incomplete combustion from burners and engines. It is known that extended exposure to these soot particles and toxic exhaust gases can cause adverse human health effects from headaches to respiratory diseases (1, 2). The formation of diesel engine-derived soot particles especially in the nanometric size range has drawn particular attention. These particles may have potentially more adverse implications to human health due to the increased reliance on diesel power over traditional spark ignition engines. Diesel engine-generated soot nanoparticles are known to have a higher fraction of harmful semivolatile species (e.g. PAHs) and nonvolatile metals, which are condensed on or within soot nanoparticles (3–5). The need to abate particulate emissions has led to the development of novel catalytic supports, where diesel soot nanoparticles are oxidatively reacted away on high-temperature

catalytic filters (6, 7). Another complimentary strategy has been to add metal additives directly into the fuel or the combustion chamber, to suppress soot emissions (8, 9). In either case, the knowledge of the oxidative propensity and kinetics are needed, particularly as it relates to recent observations on the difference between flame and diesel soot oxidative properties, described below.

The motivation for this work comes from a new experimental approach that enables us to explore the size-dependent reactivity of soot particles in a precisely controlled gas-phase environment. The present investigation is an extension of previous work dealing with the kinetics of size-selected soot nanoparticle oxidation by the use of high-temperature oxidation tandem differential mobility analyzer (HTO-TDMA) (10). A result of that work and the motivation for this study was that we found a significant difference in the oxidative properties of flame-derived soot vs diesel soot (11). In particular, we observed that for the same size particle, flame derived soot oxidizes with an activation energy of about ~ 160 kJ/mol, while soot sampled from a diesel engine was considerably lower, with an activation of about ~ 100 kJ/mol. The oxidation of metal-doped diesel soot was also studied using the same approach, where cerium oxide nanoparticles dispersed in an organic solvent were directly mixed with diesel fuel (12). We observed that the addition of cerium oxide to the fuel increased the overall oxidation rate but did not affect the activation energy.

This leaves two issues unresolved. First, why does flame soot have a much higher activation energy for oxidation? And second, why does the addition of metal either in the form of cerium oxide or lubricating oil containing metals not change the inherent activation energy for oxidation of diesel soot? One of the concerns today is that lubrication oils, which do contain metals, are in fact bypassing the piston rings and making their way to the combustion chamber (13). If so, then it is reasonable to argue that diesel soot already contains metals and that the addition of more metal as was done in the previously mentioned experiments will only increase the overall reactivity through a preexponential parameter but may not change the overall activation energy. If the latter hypothesis is correct, then that begs the question as to what happens to flame soot doped with metal.

The subject of this paper is to test the hypothesis that the oxidative differences between flame and diesel soot can be explained by the role of metal. To test this hypothesis, we have conducted a HTO-TDMA experiment of an iron doped diffusion flame and obtained size resolved kinetics of soot oxidation.

Experimental Section

The experimental setup is shown schematically in Figure 1 and consists of a diffusion burner for the formation of pure soot or iron-doped soot particles and a HTO-TDMA system for the measurement of soot oxidation rate. The details of the experiment have been outlined in our prior references (10–12). A coannular Santoro-typed burner (14) was operated with a 5 cm long laminar diffusion flame supported by ethylene fuel and air with a mixing ratio of fuel:air = 1:500. For all experiments the fuel flow rate was fixed at 110 SCCM (standard centimeter cube per minute) unless otherwise mentioned. The iron source used was iron pentacarbonyl ($\text{Fe}(\text{CO})_5$). The carbonyl was delivered by bubbling ethylene through the carbonyl liquid immersed in an ice bath (vapor pressure ~ 7 Torr). The amount of $\text{Fe}(\text{CO})_5$ added is 0.1 mol % of the fuel. A stainless steel sampling probe with an outer diameter of 1.25 cm was horizontally fixed on the flame tip

* Corresponding author e-mail: mrz@umd.edu.

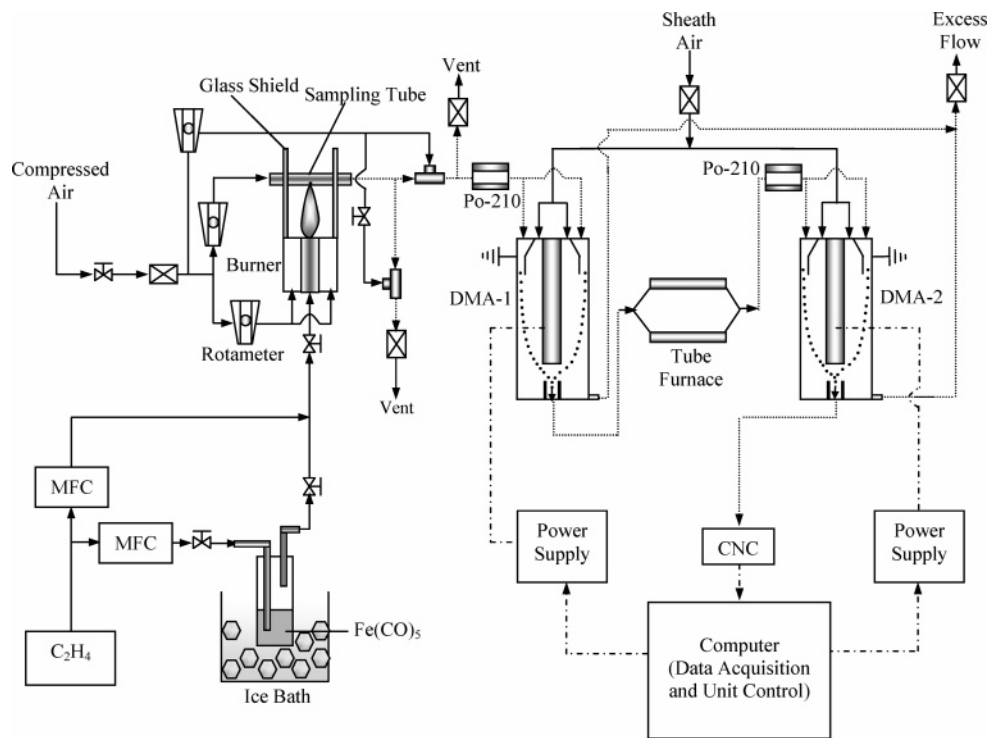


FIGURE 1. Schematic diagram of the experimental apparatus. The solid line indicates the fuel and air path, and the dotted line indicates the soot aerosol path through HTO-TDMA. Dot-dash line indicates electrical connection for data acquisition and unit control.

with an orifice of 0.1 cm in diameter (15). A flow of carrier gas through the tube serves to create a slight negative pressure, which rapidly draws, quenches, and dilutes the aerosol. The sampled soot nanoparticles were then rapidly diluted by using an ejector with a designed dilution ratio of 1:50. The controlled dilution air is supplied to the diluter via a critical orifice installed inside the ejector.

The sampled soot nanoparticles were introduced into the HTO-TDMA described in detail elsewhere (10). Briefly, aerosol is passed through a radioactive ionizing source (Po-210), which provides the soot nanoparticles with a Boltzmann charge distribution. The first differential mobility analyzer-1 (DMA-1) passes monodisperse aerosol particles with three fixed operating voltages, corresponding to equivalent electrical mobility diameters of 40, 93, and 130 nm. These three initial particle sizes were selected to compare with prior studies of flame and diesel soot oxidation (10–12). The monodisperse soot nanoparticles selected from DMA-1 were then introduced into a quartz tube (1 cm diameter \times 30 cm heating length) enclosed in a tube furnace, where the temperature is varied from room temperature to 1000 °C with a residence time of \sim 1.3 s. After passing through the oxidizing furnace the aerosol is again exposed to another radioactive ionizing source (Po-210) to recharge the particles as the heated particles tend to lose their charges upon heating. As a final step, DMA-2 combined with condensation nucleus counter (CNC) scans the evolution of the resulting size distribution after oxidation, to obtain the extent of shrinkage.

For chemical analysis of the soot nanoparticles, a Laser Microprobe Mass Spectrometry (LMMS) was used (16). For sample preparation, soot particles are electrostatically collected on a quartz window. The quadrupled pulsed YAG laser beam (266 nm) is focused through the particle-deposited quartz window, which was held in a vacuum of 10^{-4} Pa. Irradiation fluxes of 10–20 MW/cm² cause partial evaporation and ionization of the soot. The ionized species are detected with a time-of-flight mass spectrometer with a mass range of 1–5500 u.

Results and Discussion

It is well-known that iron additives in fuel play the role of a soot suppressant (17). To verify the effect of iron addition on the resulting soot nanoparticles, we measured soot particle size distributions (PSDs) using a differential mobility particle sizer (18) before and after iron loading. For the series of experiments without iron doping, the total C₂H₄ fuel flow was fixed at 110 SCCM. For the iron-doping case, we used 100 SCCM C₂H₄ fuel flow combined with 10 SCCM C₂H₄ bubbled flow through Fe(CO)₅ liquid to keep a constant total C₂H₄ flow rate. Figure 2 presents the PSD of soot before and after iron doping. The geometric mean diameters are found to be 76 and 79 nm and geometric standard deviations 2.24 and 2.10 for pure and iron-doped soot particle cases, respectively. The iron evidently has no effect on the mean size and size distribution, with the possible exception that at the very fine range of our measurement where there might be a small nuclei mode appearing in the iron doped case. The most obvious difference in the two size distributions is soot suppression of a factor of 2 observed when iron is added. This is presumably because metal particles are interfering with the inception of soot particles in the early stage of the flame and simultaneously acting as a catalyst for accelerating soot oxidation and burnout processes in the hot flame zone. However, the overall effect of a small iron addition to soot particle formation in the current flame seems to be negligible.

In flames the iron has been observed in various forms depending on the extent of iron loading. Zhang and Megaridis (19) claimed that pure iron (Fe) is present within the soot particle matrix collected above the ethylene/air nonpremixed flame with a ferrocene additive. On the other hand, Charalampopoulos et al. (20) analyzed iron-doped flame soot particles using X-ray photoelectron spectroscopy and found that the iron is present in the form of Fe₂O₃ within the soot matrix. We collected polydisperse soot particles before and after iron doping, and the chemical composition of soot particles collected were analyzed using laser microprobe mass spectrometry (LMMS). Figure 3 presents a typical positive ion spectra obtained. One can see the signature from carbon

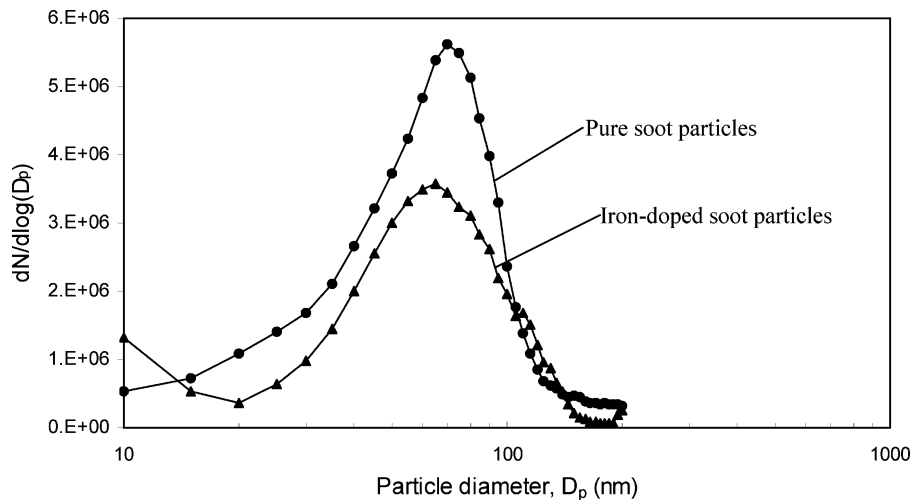


FIGURE 2. Particle size distributions for original soot particles with and without iron-doping case.

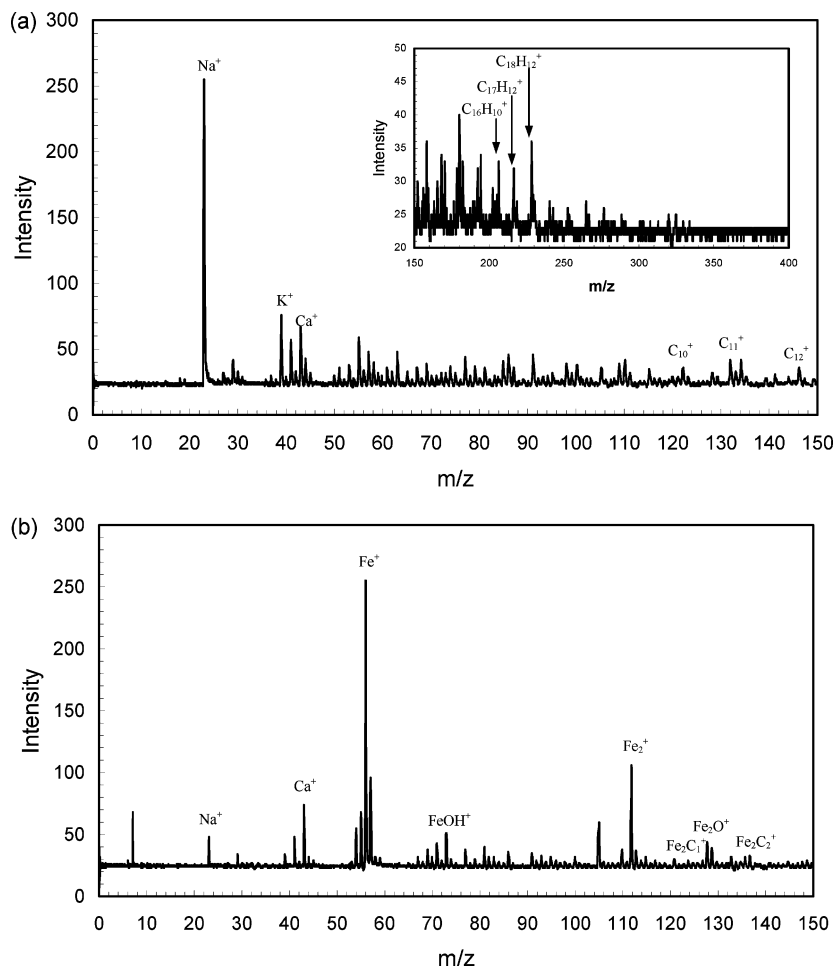


FIGURE 3. Mass spectra of soot particles (a) before and (b) after iron doping.

clusters ($m/z = 120$ [C_{10}^+], 132 [C_{11}^+], 144 [C_{12}^+] etc.) and various PAHs ($m/z = 202$ [$C_{16}H_{10}^+$], 216 [$C_{17}H_{12}^+$], 228 [$C_{18}H_{12}^+$] etc.) for pure soot particles as seen in Figure 3a. Relatively strong peaks of Na^+ , K^+ , and Ca^+ are presumably originating from contamination of the quartz window preparation during the drying process in a ceramic tube furnace. For the iron-doped soot particles (Figure 3b), there exists strong iron peaks ($m/z = 54, 56, 57, \text{ and } 58$ [Fe and stable Fe isotopes]) and possible iron clusters ($m/z = 112$ [Fe_2^+]). Identified in the LMMS spectra are possible $FeOH^+$ ($m/z = 73$), Fe_2O^+ ($m/z = 128$), and $Fe_2C_x^+$ (where $x = 1, 2$; $m/z = 124, 136,$

respectively). The presence of these peaks does not necessarily require that the iron compounds are present in these forms in the sample, since it is possible that the species could form by collision in the laser induced plasma.

However, signatures for FeO^+ , Fe_2O^+ , and $Fe_2O_3^+$ are relatively very weak compared with Fe^+ and Fe_2^+ . This result is also consistent with single particle mass spectrometry studies we have conducted on the fate of iron in diesel soot, where we also observed zero valence iron (3). That is not to say that iron oxide is never formed in the flame. It is possible that iron oxide may be converted into pure iron by carbon-

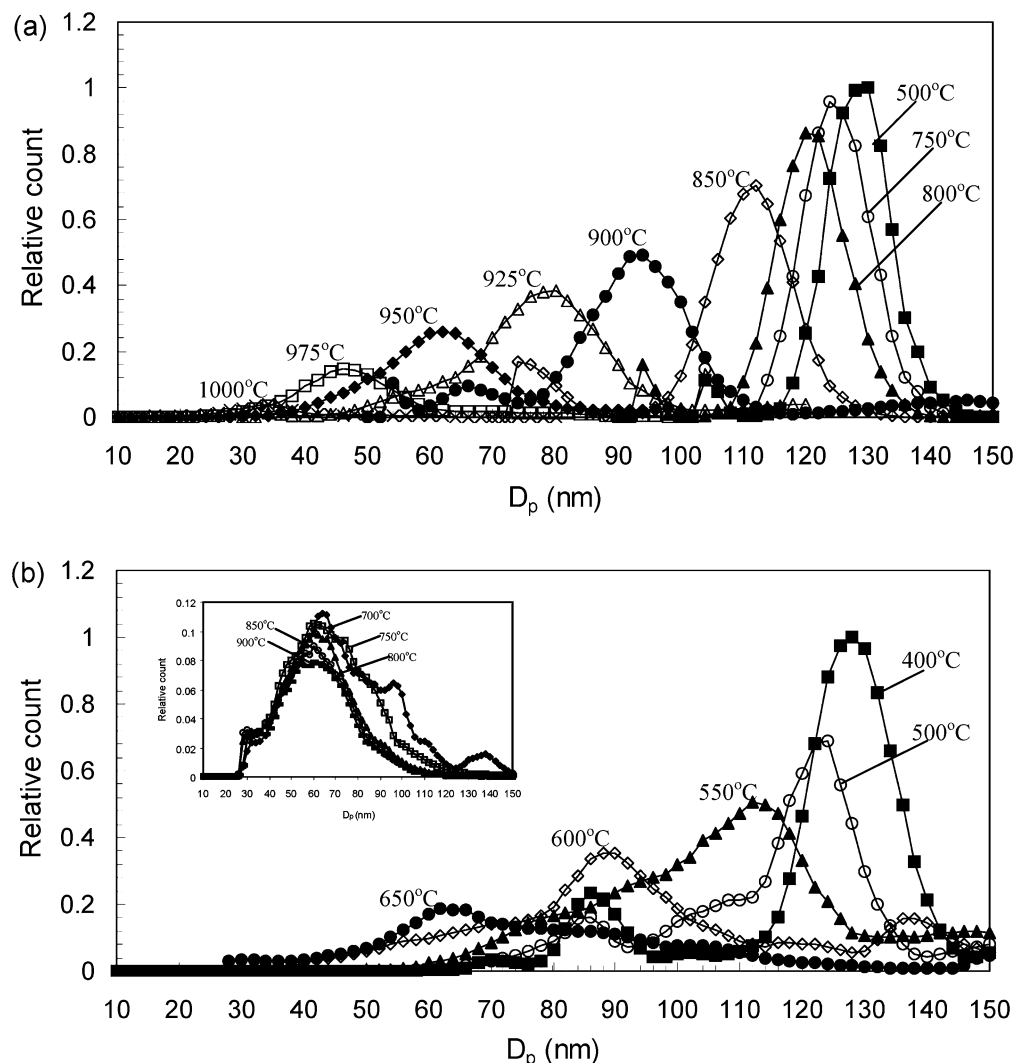


FIGURE 4. HTO-TDMA results for soot oxidation in air for various temperatures from 400 to 1000 °C: (a) non-iron-doped soot nanoparticles and (b) iron-doped soot nanoparticles.

thermal reduction, $Fe_xO_y + yC \rightarrow xFe + yCO$ (21). With sufficient iron loading, iron oxide may nucleate with the possibility of separation of iron oxide from soot matrix (22). However, for these experiments where there is small quantities (~3%) of iron present we think that considerable elemental iron is present. The other conclusion is that for the purpose of this investigation which serves to compare the behavior of diesel and flame soot, the state of the iron is indistinguishable.

On the basis of our observation of the iron seeding effect on physical and chemical properties of soot particles, we conducted a series of HTO-TDMA measurements to explore the catalytic characteristics of iron within the soot matrix. The representative HTO-TDMA measurement for the 130 nm initial particle size with and without iron-doped soot is presented in Figure 4. For pure soot particles as shown in Figure 4a, the particle size changed by less than 1% for temperatures up to 500 °C and is likely due to evaporation of volatile materials condensed on the soot particles. This fact is verified by employing nitrogen carrier gas instead of air (10). Above 500 °C, the soot particles undergo significant oxidation and higher extents of oxidation with increasing temperature for fixed residence time. Careful observation of the profiles in Figure 4a also shows small satellite peaks. These correspond to the small fraction of particles that have two charges and are larger particles with the equivalent mobility diameter (23). The decrease in number density with

increasing temperature can be attributed to thermophoretic deposition of soot particles to the reactor wall. The thermophoretic loss of soot particles is promoted with increasing temperature due to the higher temperature gradient. With increasing reactor temperature a greater fraction of the aerosol is lost to the walls at the exit of the reactor. However, since thermophoretic velocity is particle size independent we expect no changes to the resulting size distribution. Since our analysis relies on size change and does not depend on number concentration, these losses have no impact on our data analysis. Figure 4b shows the evolution of size distribution of iron-doped soot nanoparticles at various oxidation temperatures. Unlike the pure soot particles, the mean size of the iron-doped soot particles decreased significantly even at 500 °C. At the higher temperature range (700 °C–900 °C), particle shrinkage ceases as shown in the inserted graph. Here we believe we have completely burned out the soot leaving behind iron which also has presumably been oxidized. If we assume that the iron nanoparticles are oxidized to Fe_2O_3 , and using the bulk densities of iron and iron oxide with 7.86 and 5.18 g/cm³, respectively, we can work backward to determine the effective size of the original iron constituent. In this way the 60 nm peak corresponds to a volume equivalent diameter of 41 nm for pure iron. Working back further we can determine that the relative volume loading from the original 131 nm soot particle we started at gives a ~3% iron volume loading relative to soot mass.

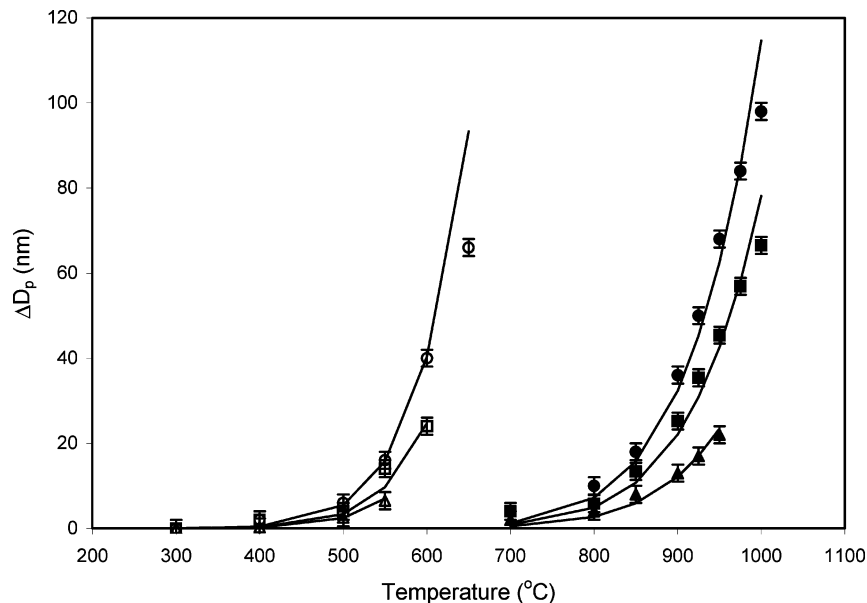


FIGURE 5. Comparison of particle size change as a function of temperature for the 40 nm (triangles), 93 nm (squares), and 130 nm (circles) initial sizes of non-iron-doped (solid symbols) and iron-doped (open symbols) soot nanoparticles. Solid lines are the fitted models based upon the kinetic parameters of Arrhenius equation as shown in Table 1.

TABLE 1. Fitted Kinetic Parameters

parameter	Higgins et al. (11) and Jung et al. (12)				current study			
	diesel particles			cerium-doped diesel particles		diffusion flame soot particles		
	10% load	50% load	75% load	25 ppm	100 ppm	non-iron doping	iron doping	
E_a [kJ mol ⁻¹]	114	109	108	107	102	162 ± 3	116 ± 3	
A_{40} [nm K ^{-1/2} s ⁻¹]	8.8 × 10 ⁴	3.1 × 10 ⁴	2.6 × 10 ⁴	6.6 × 10 ⁵	5.0 × 10 ⁵	1.2 × 10 ⁷	8.0 × 10 ⁶	
A_{93} [nm K ^{-1/2} s ⁻¹]	7.7 × 10 ⁴	4.5 × 10 ⁴	3.8 × 10 ⁴	7.3 × 10 ⁵	7.0 × 10 ⁵	2.2 × 10 ⁷	1.1 × 10 ⁷	
A_{130} [nm K ^{-1/2} s ⁻¹]	11.2 × 10 ⁴	5.4 × 10 ⁴	4.8 × 10 ⁴	8.6 × 10 ⁵	5.8 × 10 ⁵	3.2 × 10 ⁷	1.8 × 10 ⁷	

The rate of the particle size shrinkage as measured by HTO-TDMA corresponds to the rate of mass loss of materials and can be related to the reaction rate constant for soot oxidation. The temperature-dependent size decrease rate is assumed to obey a modified Arrhenius equation as outlined in detail in our prior work (10)

$$\dot{D}_p = -A_{nm} T^{1/2} \exp\left[-\frac{E_a}{RT}\right] \quad (1)$$

where A_{nm} is the size-dependent preexponential factor, T is the temperature, E_a is the size-independent activation energy, and R is the gas constant.

To relate the size decrease rate measured by the HTO-TDMA system with the Arrhenius equation, eq 1 is integrated over the length of the heating zone in the tube furnace as follows

$$\Delta D_p = \int_0^X \frac{\dot{D}_p(x)}{u(x)} dx \quad (2)$$

where x is a horizontal position in the tube, X is the length of the tube, and u is the flow velocity, which is calculated as below

$$u(x) = \frac{4}{3} u_m \frac{T(x)}{T_o} \quad (3)$$

where $4/3 u_m$ is the peak flow velocity of carrier gas calculated from volume flow rate and the cross sectional area of the flow tube under the assumption of laminar flow.

Figure 5 presents the size decrease measured by the HTO-TDMA system (symbols) and the fit to eqs 1–3. The open circle data representing the iron-doped case clearly show a much reduced on-set temperature relative to the undoped case (solid symbols). Table 1 summarizes the kinetic parameters (A_{40} , A_{93} , A_{130} , and E_a) found by a best fit to the experimental data, which are also plotted in Figure 5 as the solid lines. We first note a significant decrease in the activation energy from 162 ± 3 kJ/mol for the pure soot to 116 ± 3 kJ/mol for the iron-doped case. The preexponential factors for the iron-doped soot particles are slightly smaller (factor of 2) as compared to the undoped case. However, due to the sensitivity of the fit to the activation energy it is difficult to assess if this is a real effect or simply an artifact of the fit. The absolute values of the A factor are consistent with the data taken in a previous study from our group (10). The slight size dependent rates observed, whereby the larger particles have an increased apparent oxidation rate has been discussed in our prior work and have been attributed to an assumption made of constant effective density. One also notes that there is a large difference in preexponential factors between diesel and flame soot particles. This observation, which we have reported on previously (11), is presumably related to some inherent chemical difference between flame and diesel generated soot which has not yet to be addressed adequately. For example hydrogen content is generally higher, and diesel soot also generally contains a significant amount of sulfur and nitrogen (24).

Since the volume fraction of metal content in the current flame soot matrix (~3% volume fraction) is larger than that of diesel soot (~1% volume fraction), we reduced the iron addition down by a factor of 5 (~0.02 mol % of the fuel) to

observe the effect of the amount of iron loading on the activation energy and A factor. For comparison, 93 nm initial iron-doped flame soot particles were selected for HTO-TDMA measurement. The kinetic parameters found were $161 \pm 3 \text{ kJ mol}^{-1}$ [$2.2 \times 10^7 \text{ nm K}^{-1/2} \text{ s}^{-1}$], $133 \pm 3 \text{ kJ mol}^{-1}$ [$1.2 \times 10^7 \text{ nm K}^{-1/2} \text{ s}^{-1}$], and $116 \pm 3 \text{ kJ mol}^{-1}$ [$1.1 \times 10^7 \text{ nm K}^{-1/2} \text{ s}^{-1}$] for non-iron loading, 0.02 mol % iron loading, and 0.1 mol % iron loading cases, respectively. These results are consistent with the hypothesis that small quantities of metal seeding in soot matrix increases the reactivity of the resulting soot nanoparticles by significantly decreasing their activation energy.

Discussing the Role of Metal. The premise of this work was to rationalize why flame soot and diesel soot show very different temperature sensitivity to oxidation (i.e. activation energy). Prior observations are that the addition of metal additives to diesel results in a decrease in soot emissions, which can be attributed to either suppressing soot inception and growth or promoting oxidation in the combustion chamber. Our own prior studies on oxidation kinetics have shown that adding cerium oxide, a known catalyst, to diesel fuel increased the oxidation rate but did not affect the activation energy (12). Similarly, the addition of lubrication oil, which contains significant quantities of metal, increased the oxidation rate but did not affect the activation energy (25). All these results point to an indirect conclusion that diesel soots already contain metals that catalyze the oxidation of soot.

A more direct determination of this hypothesis and the subject of this paper are then to add metals to ordinarily metal-free flame soot. The results showed that indeed the activation energy for oxidation dropped very close to the values observed for nascent diesel soot. This suggests that the primary difference in the thermal-oxidative behavior between flame and diesel soot may come from the metals that are already in diesel soot. These results suggest that those researchers interested in modeling soot emissions from engines with detailed chemical kinetics models of the combustion process still need to incorporate oxidation models that account for this effect.

In this paper we explore the hypothesis that the lower activation energy for soot oxidation observed for diesel engine derived particles versus flame derived soot may be associated with the catalytic role of metals coming from lubricating oil. To test this hypothesis, we doped a flame with iron and found that indeed addition of iron to a flame reduced the activation energy significantly from $\sim 162 \pm 3 \text{ kJ/mol}$ to $\sim 116 \pm 3 \text{ kJ/mol}$ and in line with diesel engine generated soot with an activation energy $\sim 110 \text{ kJ/mol}$. These results are consistent with the idea that small quantities of metals during diesel combustion may play an important role in soot abatement.

Literature Cited

- (1) Health Assessment Document for Diesel Engine Exhaust, 2002, EPA/600/8-90/057F.
- (2) Aust, A. E.; Ball, J. C.; Hu, A. A.; Lighty, J. S.; Smith, K. R.; Straccia, A. M.; Veranth, J. M.; Young, W. C. Particle characteristics responsible for effects on human lung epithelial cells. *Res. Report-Health Effects Institute* **2002**, 110, 1.
- (3) Lee, D.; Miller, A.; Kittelson, D. B.; Zachariah, M. R. Characterization of metal-bearing diesel nanoparticles using single particle mass spectrometry. *J. Aerosol Sci.* **2005**, in press.
- (4) Skillas, G.; Qian, Z.; Baltensperger, U.; Matter, U.; Burtscher, H. The influence of additives on the size distribution and composition of particles produced by diesel engines. *Combust. Sci. Technol.* **2000**, 154(1), 259.
- (5) Wang, Y. F.; Huang, K. L.; Li, C. T.; Mi, H. H.; Luo, J. H.; Tsai, P. J. Emissions of fuel metals content from a diesel vehicle engine. *Atmos. Environ.* **2003**, 37, 4637.
- (6) Baumgard, K. J.; Kittelson, D. B. The Influence of a ceramic particle trap on the size distribution of diesel particles. *SAE Pap.* **1985**, No. 850009.
- (7) Lepperhoff, G.; Kroon, G. Impact of particulate traps on the hydrocarbon fraction of diesel particles. *SAE Pap.* **1985**, No. 850013.
- (8) Kasper, M.; Sattler, K.; Siegmann, K.; Matter, U.; Siegmann, H. C. The influence of fuel additive on the formation of carbon during combustion. *J. Aerosol Sci.* **1999**, 30(2), 217.
- (9) Miyamoto, N.; Hou, Z.; Ogawa, H. Catalytic effects of metallic fuel additives on oxidation characteristics of trapped diesel soot. *SAE Pap.* **1988**, No. 881224.
- (10) Higgins, K. J.; Jung, H.; Kittelson, D. B.; Roberts, J. T.; Zachariah, M. R. Size-selected nanoparticle chemistry: kinetics of soot oxidation. *J. Phys. Chem. A* **2002**, 106, 96.
- (11) Higgins, K. J.; Jung, H.; Kittelson, D. B.; Roberts, J. T.; Zachariah, M. R. Kinetics of diesel nanoparticle oxidation. *Environ. Sci. Technol.* **2003**, 37, 1949.
- (12) Jung, H.; Kittelson, D. B.; Zachariah, M. R. The influence of engine lubricating oil on kinetics of diesel particle oxidation. *Combust. Flame* **2005**, in press.
- (13) Kyto, M.; Askko, P.; Nylund, N. O.; Niemi, A. Effect of lubricant on particulate emissions of heavy-duty diesel engines. *SAE Pap.* **2002**, No. 2002-01-2770.
- (14) Santoro, R. J.; Semerjian, H. G.; Dobbins, R. A. Soot particle measurements in diffusion flames. *Combust. Flame* **1983**, 51, 203.
- (15) Kasper, M.; Siegmann, K.; Sattler, K. Evaluation of an in-situ sampling probe for its accuracy in determining particle size distributions from flames. *J. Aerosol Sci.* **1997**, 28(8), 1569.
- (16) Fletcher, R. A.; Dobbins, R. A.; Chang, H.-C. Mass spectrometry of particles formed in a deuterated ethane diffusion flame. *Anal. Chem.* **1998**, 70(13), 2745.
- (17) Linteris, G. T.; Katta, V. R.; Takahashi, F. Experimental and numerical evaluation of metallic compounds for suppressing cup-burner flames. *Combust. Flame* **2004**, 138, 78.
- (18) Fissan, H.; Helsper, C.; Thielen, H. J. Determination of particle size distribution by means of a nanometer aerosol sampler. *J. Aerosol Sci.* **1983**, 14, 354.
- (19) Zhang, J.; Megaridis, C. M. Soot suppression by ferrocene in laminar ethylene/air nonpremixed flames. *Combust. Flame* **1996**, 105, 528.
- (20) Charalampopoulos, T. T.; Hahn, D. W.; Chang, H. Role of metal additives in light scattering from flame particulates. *Appl. Optics* **1992**, 31, 6519.
- (21) Sturgeon, R. E.; Chakrabarti, C. L.; Langford, C. H. Studies on the mechanism of atomic formation in graphite furnace atomic absorption spectrometry. *Anal. Chem.* **1976**, 48, 1792.
- (22) Yang, G.; Teague, S.; Pinkerton, K.; Kennedy, I. M. Synthesis of an ultrafine iron and soot aerosol for the evaluation of particle toxicity. *Aerosol Sci. Technol.* **2001**, 35, 759.
- (23) Kim, S. H.; Woo, K. S.; Liu, B. Y. H.; Zachariah, M. R. Method of measuring the charge distribution of nanosized aerosols. *J. Colloid Inter. Sci.* **2005**, 282(1), 46.
- (24) Ahlstrom, A. F.; Odenbrand, C. U. I. Combustion characteristics of soot deposits from diesel engines. *Carbon* **1989**, 27(3), 475.
- (25) Jung, H.; Kittelson, D. B.; Zachariah, M. R. The influence of engine lubricating oil on diesel nanoparticle emissions and kinetics of oxidation. *SAE Pap.* **2003**, No. 2003-01-3179.

Received for review July 27, 2004. Revised manuscript received February 21, 2005. Accepted March 29, 2005.

ES048828Z